



Quantifying national, state, and oil/gas field methane emissions and trends in the U.S. (2019-2024) through high resolution inversion of satellite observations

Lucas A. Estrada¹, Daniel J. Jacob¹, Megan He¹, James D. East^{1,2}, Daniel J. Varon^{3,4}, Nicholas Balasus¹,
5 Sarah E. Hancock¹, Melissa Sulprizio¹, Kevin W. Bowman⁵, John R. Worden⁵, Emily Reidy⁶, Benjamin
R. K. Runkle⁷

¹School of Engineering and Applied Science, Harvard University, Cambridge, Massachusetts, 02134, USA

²International Methane Emissions Observatory (IMEO), United Nations Environment Programme (UNEP), Paris, France

10 ³Massachusetts Institute of Technology, Department of Aeronautics and Astronautics, Cambridge, MA, 02139, USA

⁴Massachusetts Institute of Technology, Institute for Data, Systems, and Society, Cambridge, MA, 02139, USA

⁵Jet Propulsion Laboratory, California Institute of Technology, Pasadena, CA, 91011, USA

⁶ExxonMobil Technology and Engineering Company, Spring, TX, USA

⁷Department of Biological and Agricultural Engineering, University of Arkansas, Fayetteville, AR, 72701, USA

15 *Correspondence to:* Lucas A. Estrada (lestrada@g.harvard.edu)

Abstract. We quantify trends of U.S. methane emissions at the national, state, and oil/gas field levels for 2019-2024 through high-resolution (up to ~25 km) analytical inversion of TROPOMI satellite observations with the open-source Integrated Methane Inversion (IMI 2.1). We find that total anthropogenic methane emissions (37 Tg a^{-1}) are 34% higher in magnitude than reported in the U.S. Environmental Protection Agency (EPA) Greenhouse Gas Inventory (GHGI) that provided prior
20 estimates for the inversion. Oil/gas emissions are 64% higher than the GHGI, consistent with previous studies. Total emissions are flat over the 2019-2024 period ($0.0 \pm 1.0\% \text{ a}^{-1}$) but this total reflects a combination of decreasing emissions from the oil/gas ($-1.1 \pm 0.9\% \text{ a}^{-1}$), coal ($-2.3 \pm 1.3\% \text{ a}^{-1}$), and rice ($-9.1\% \pm 2.0 \text{ a}^{-1}$) sectors, offset by increases in the livestock ($1.8 \pm 1.3\% \text{ a}^{-1}$) and landfill ($0.5 \pm 1.4\% \text{ a}^{-1}$) sectors. The methane intensity from the oil/gas sector continues its downward trend, from 2.3% to 1.9% over the 2019-2024 period, but unlike in previous studies we find that this trend does not simply
25 reflect an increase in production but also a decrease in emissions, demonstrating improved emission management. Over half of total U.S. emissions originate from ten states, most dominated by fuel exploitation. Emission inventories compiled by individual states do not always improve on GHGI state estimates. Methane intensities decrease for all major oil/gas fields except those with declining production.

1 Introduction

30 Methane is a strong climate forcer and has contributed approximately $0.5 \text{ }^\circ\text{C}$ of warming since the industrial revolution (Forster et al., 2021). The strong radiative effect of methane and its short atmospheric lifetime (~10 years) make it a top



policy target for mitigating near-term global temperature rise. Anthropogenic emissions are from both microbial (agriculture, waste, reservoirs) and fossil sources (oil, gas, and coal operations). The U.S. is the second largest emitter of anthropogenic methane after China (Saunio et al., 2025) with major sources from livestock, oil/gas operations, waste, and coal mining. It is one of the 160 countries that signed the Global Methane Pledge to reduce methane emissions collectively by 30% by 2030 from 2020 levels. Here, we use the open-source cloud-based Integrated Methane Inversion (IMI 2.1) software tool applied to TROPOMI satellite observations of atmospheric methane to quantify U.S. methane emissions and their trends over the 2019-2024 period at the national, state, and oil/gas field levels. Our goal is to set up a transparent system for monitoring annual emissions in support of climate agreements using publicly available satellite data and an open-source user-friendly inversion platform.

The U.S. has reported methane emission estimates annually by sector to the United Nations Framework Convention on Climate Change (UNFCCC) as part of the Greenhouse Gas Inventory (GHGI) from the U.S. Environmental Protection Agency (EPA, 2024). The GHGI for methane is provided at $0.1^{\circ} \times 0.1^{\circ}$ grid resolution (Maasakkers et al., 2023). It uses bottom-up methods based on activity data and emission factors, including additional information on large sources from the Greenhouse Gas Reporting Program (GHGRP, 2025). Inversions of atmospheric methane observations can evaluate and refine the GHGI and provide current estimates of emissions not subject to the latency in the collection of national bottom-up information but with the spatial granularity needed for sectoral assessment. As of 2025 the U.S. government has suspended its reporting to the UNFCCC, making inversion of atmospheric observations all the more important to update annual national emissions.

Many studies have previously derived methane emissions in the U.S. from observations of atmospheric concentrations from surface sites and aircraft. Most have used inverse methods in which a best posterior estimate of emissions is obtained by Bayesian optimization combining the observations, an atmospheric transport model to relate the observations to emissions, and a prior bottom-up emission estimate. Early inversion studies consistently found that the EPA and EDGAR (Crippa et al., 2024) bottom-up inventories underestimated U.S. methane emissions (Kort et al., 2008; Miller et al., 2013). Regional analyses highlighted large discrepancies in livestock and oil/gas sources (Zhao et al., 2009; Karion et al., 2013; Alvarez et al., 2018).

Space-based observations from SCIAMACHY (2003-2012), GOSAT (2009-present), and TROPOMI (2018-present) have expanded the spatial coverage and continuity of methane observations, enabling regional and continental inversions worldwide (Jacob et al., 2016; Houweling et al., 2017; Jacob et al., 2022). Kort et al. (2014) showed that the SCIAMACHY instrument could identify methane hotspots and quantify emissions in the U.S. Four Corners region. Buchwitz et al. (2017) estimated emissions in the Four Corners region by combining SCIAMACHY and GOSAT observations. Turner et al. (2015) used GOSAT to infer a 60% underestimate of U.S. emissions in EDGAR and the GHGI. TROPOMI removed some of the



70 limitations of SCIAMACHY (low resolution) and GOSAT (sparse coverage) with its high spatial resolution ($5.5 \times 7 \text{ km}^2$ at nadir) and global daily coverage (Lorente et al., 2021). TROPOMI-based studies of the Permian oil/gas basin found GHGI emissions to be underestimated by a factor of 2-4 (Schneising et al., 2020; Zhang et al., 2020, Liu et al., 2021; Shen et al., 2022; Varon et al., 2023). Nesser et al. (2024) conducted a continental-scale inversion at $\sim 25 \text{ km}$ resolution using TROPOMI observations to uncover a 50% underestimate in GHGI-reported landfill emissions.

75 Long-term records of surface and satellite observations have also been used to infer trends in U.S. emissions. Schneising et al. (2014) found rising emissions in the Bakken and Eagle Ford oil/gas basins during the late 2000s from analysis of SCIAMACHY observations. Turner et al. (2016) found a 30% rise in U.S. emissions from 2002 to 2014 using GOSAT and surface data, though Bruhwiler et al. (2017) attributed the trend to meteorological variability and background errors, and Sheng et al. (2018) revised the analysis to infer a sustained rise of $2.5\% \text{ a}^{-1}$ in U.S. emissions for 2010-2016. Lan et al. (2019) also detected a rise at NOAA surface sites during 2006-2015, but with lower magnitude ($0.7\% \text{ a}^{-1}$). A 2010-2015 inversion of GOSAT data found a $0.4\% \text{ a}^{-1}$ increase in US emissions driven by the oil/gas sector (Maasakkers et al., 2021), while a 2010-2017 inversion found an emissions peak in 2014 followed by a downturn, suggesting a turning point in U.S. emissions (Lu et al., 2022).

85 Little work has been done to diagnose trends in U.S. emissions past 2019. The TROPOMI record starting in May 2018 is now sufficiently long to enable trend analyses. A new blended TROPOMI+GOSAT product (Balasus et al., 2023) removes aerosol and surface reflectivity artifacts present in previous retrievals (Barré et al., 2021; Somkuti et al., 2025). IMI analysis with this product detected strong seasonality in the Permian but no long-term trend (Varon et al., 2025). Global inversions covering 2019-2024 found no significant trends in U.S. emissions (He et al., 2025; Pendergrass et al., 2025), but the coarse resolution ($2^\circ \times 2.5^\circ$) of these studies prohibited detailed attribution.

90 Here, we use the TROPOMI+GOSAT retrieval of Balasus et al. (2023) to quantify annual emissions in the contiguous U.S. (CONUS) and their trends for six years (2019-2024) at up to $\sim 25 \text{ km}$ ($0.25^\circ \times 0.3125^\circ$) resolution with the IMI version 2.1 (Varon et al., 2022; Estrada et al., 2025) and the gridded EPA GHGI (Maasakkers et al., 2023) as prior estimate. The IMI is an open-source, cloud-based software tool that can provide transparent reporting of emissions. Annual results are visualized on a custom dashboard (laestrada.github.io/conus_emissions_viz/). The system has been adapted to the U.S. Greenhouse Gas (U.S. GHG Center, 2025) to allow emissions updates on an annual basis. We compare our results to the mean emissions and trends of the GHGI, further compare to independent state emission inventories, and examine trends in methane intensities from the oil/gas sector nationally and for individual oil/gas production fields.

2 Data and methods

We use TROPOMI satellite observations of atmospheric column concentrations and a chemical transport model (GEOS-Chem) to infer methane emissions at up to ~25 km resolution for CONUS annually for six years (2019-2024). This process is achieved with an analytical inversion using the cloud-based, Integrated Methane Inversion (IMI) framework over the domain of Figure 1. CONUS accounts for 98% of U.S. emissions (Maasakkers et al., 2016). The prior estimate of anthropogenic emissions is from the GHGI (Maasakkers et al., 2023). An ensemble of 42 inversions with varied hyperparameters is used to produce a best estimate and to bracket uncertainties.

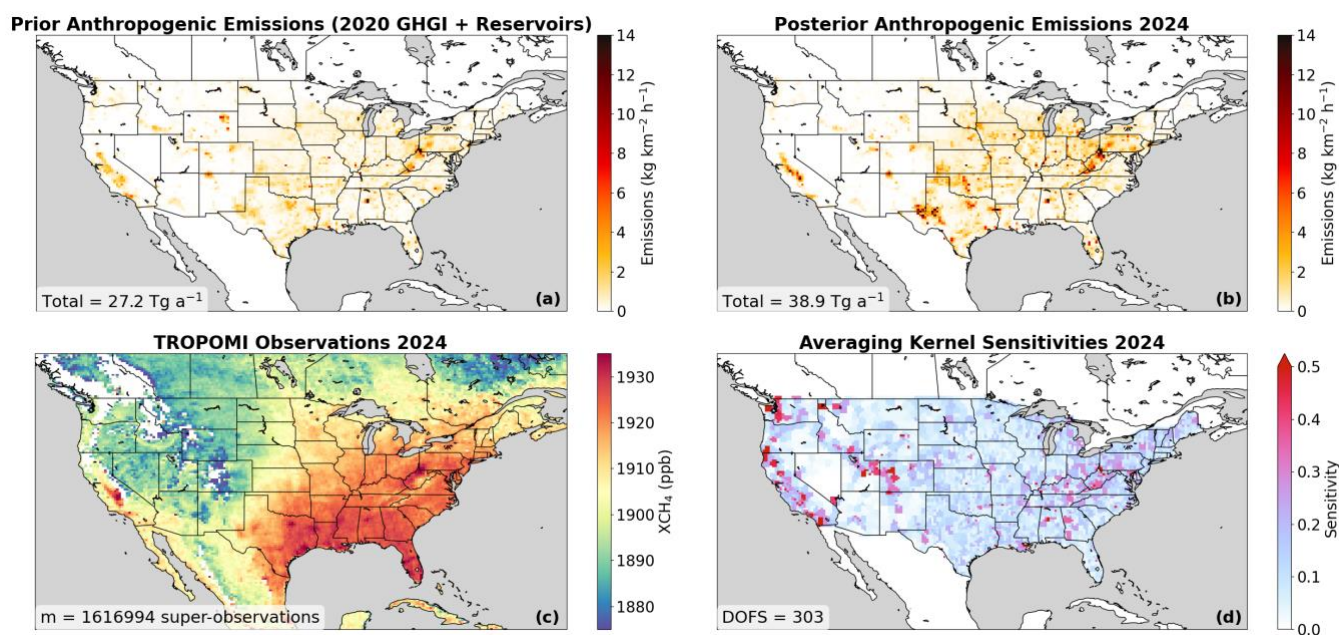


Figure 1: CONUS anthropogenic methane emissions, TROPOMI observations, and inversion averaging kernel sensitivities for 2024. Values are annual means. **(a)** Prior emissions from the EPA Greenhouse Gas Inventory (GHGI) with added contribution from hydroelectric reservoirs (Delwiche et al., 2022). Total emission is inset. **(b)** Posterior anthropogenic emissions from the mean of our inversion ensemble. **(c)** TROPOMI observations of dry column methane mixing ratios (X_{CH_4}), averaged on the $0.25^\circ \times 0.3125^\circ$ GEOS-Chem grid as hourly super-observations. Low values reflect topography. White grid cells have no observations. Total number of super-observations is inset. **(d)** Averaging kernel sensitivities for the inversion (diagonal elements of the averaging kernel matrix) on the state vector grid. The sum of averaging kernel sensitivities, representing the degrees of freedom for signal (DOFS), is inset.

2.1 Analytical inversion with the IMI

We apply the IMI (version 2.1) to infer emissions by minimizing the Bayesian cost function with normal error statistics (Brasseur and Jacob, 2017):

$$J(\mathbf{x}) = (\mathbf{x} - \mathbf{x}_A)^T \mathbf{S}_A^{-1} (\mathbf{x} - \mathbf{x}_A) + \gamma (\mathbf{y} - \mathbf{K}\mathbf{x})^T \mathbf{S}_0^{-1} (\mathbf{y} - \mathbf{K}\mathbf{x}), \quad (1)$$

where \mathbf{x} is the state vector of emissions and boundary conditions, \mathbf{x}_A is the prior estimate, \mathbf{y} is the vector of observations, $\mathbf{K} = \partial \mathbf{y} / \partial \mathbf{x}$ is the Jacobian matrix relating emissions to concentrations in GEOS-Chem, \mathbf{S}_A is the prior error covariance



matrix, \mathbf{S}_0 is the observational error covariance matrix, and γ is a regularization parameter to prevent overfit to the observations. \mathbf{S}_A and \mathbf{S}_0 are taken as diagonals for lack of better information, and $\gamma < 1$ is needed to correct for error correlation between super-observations that is not accounted for in \mathbf{S}_0 . We use the blended TROPOMI+GOSAT observation product (Balasus et al., 2023) which corrects the operational TROPOMI data for albedo and aerosol biases. The number of observations ingested each year varies from 7.6 to 10.4 million. We average observations over the $0.25^\circ \times 0.3125^\circ$ GEOS-Chem grid for each orbit to create super-observations (Eskes et al., 2003), where the reduction in retrieval error from averaging accounts for error correlations as described by Z. Chen et al. (2023). Hereafter, we refer to the blended TROPOMI+GOSAT dataset as TROPOMI.

The optimal estimate, $\hat{\mathbf{x}}$, can be derived analytically by solving $dJ/d\mathbf{x} = \mathbf{0}$ (Rodgers, 2000; Brasseur and Jacob, 2017), yielding:

$$\hat{\mathbf{x}} = \mathbf{x}_A + (\gamma \mathbf{K}^T \mathbf{S}_0^{-1} \mathbf{K} + \mathbf{S}_A^{-1})^{-1} \gamma \mathbf{K}^T \mathbf{S}_0^{-1} (\mathbf{y} - \mathbf{K} \mathbf{x}_A). \quad (2)$$

The analytical solution provides explicit error characterization through $\hat{\mathbf{S}}$, the posterior error covariance matrix:

$$\hat{\mathbf{S}} = (\gamma \mathbf{K}^T \mathbf{S}_0^{-1} \mathbf{K} + \mathbf{S}_A^{-1})^{-1}. \quad (3)$$

The averaging kernel matrix $\mathbf{A} = \partial \hat{\mathbf{x}} / \partial \mathbf{x} = \mathbf{I} - \hat{\mathbf{S}} \mathbf{S}_A^{-1}$ describes the sensitivity of the inversion to the true state. The diagonal elements of \mathbf{A} , a_{ii} , are called averaging kernel sensitivities and measure the ability of the observations to infer emissions on the native state vector grid independently of the prior estimate, ranging from 0 (no ability) to 1 (complete ability). Emissions can still be quantified from the observations when averaging kernel sensitivities are low by spatial aggregation. The sum of averaging kernel sensitivities (trace of \mathbf{A}) defines the degrees of freedom for signal (DOFS), estimating the total independent number of pieces of information from the observations.

The posterior error covariance matrix $\hat{\mathbf{S}}$ does not account for uncertainties in inversion hyperparameters (prior error standard deviation, observational error standard deviation, regularization parameter, error distribution, etc.) which dominate the overall error (Z. Chen et al., 2022). As a more conservative estimate of uncertainties on our posterior emission estimates, we generate an ensemble of estimates with varied inversion hyperparameters, considering both normal and lognormal probability density functions (pdfs) for the prior emission error estimates (Table 1). Lognormal error pdfs may better characterize the heavy tail of emissions, particularly for the oil/gas sector (Yuan et al., 2015; Cui et al., 2019), and have the advantage of enforcing positivity in the solution. Lognormal error pdfs are accommodated in Eq. 1 by solving for $\ln \mathbf{x}$ instead of \mathbf{x} , which makes the forward model non-linear and requires solving for $\ln \hat{\mathbf{x}}$ iteratively. We solve this problem with the Levenberg-Marquardt algorithm (Z. Chen et al., 2022). The optimization is then for the median of \mathbf{x} rather than the mean, which requires median-mean conversions as described by Hancock et al. (2025). To minimize biases from the boundary conditions, we optimize each domain edge as part of the inversion following Nesser et al. (2025). From the combinations of inversion hyperparameters in each column of Table 1, we generate an ensemble of 36 normal and 6 lognormal estimates.



150 These combinations were chosen such that the prior terms of the cost function roughly match (between 0.5 and 1.5 normalized) the expected chi-square value, indicating a successful fit (Lu et al., 2022). We report the mean from the ensemble members (equal weighting for normal and lognormal pdfs) as our best estimate and the range as our uncertainty. We calculate our trends using Ordinary Least Squares (OLS) regression on the mean estimates for each individual year and report the corresponding standard error from the regression.

155 **Table 1: Hyperparameters of the inversion ensemble**

Hyperparameter	Normal error pdf	Lognormal error pdf
Prior error standard deviation on CONUS emissions^a	[0.5, 0.75, 1.0]	[1.5, 2.0, 2.5]
Prior error standard deviation on non-CONUS emissions^b	0.5	0.5
Boundary condition error standard deviation (ppb)	[5, 10, 15]	10
Observational error standard deviation (ppb)	[10, 15]	15
Regularization parameter γ	[0.1, 0.2]	[0.1, 0.2]

^a For state vector elements in CONUS; fractional error standard deviation for normal error pdf inversions, geometric standard deviation for lognormal error pdf inversions.

^b Fractional error standard deviation for state vector elements outside CONUS. The prior error for these elements follows a normal distribution in all cases.

2.2 Forward Model

160 We apply the GEOS-Chem chemical transport model (version 14.4.1) as the forward model to relate emissions to atmospheric concentrations (Maasakkers et al., 2019) as expressed by the Jacobian matrix \mathbf{K} in Eq. 1. The model is driven by NASA GMAO GEOS-FP meteorological fields at $0.25^\circ \times 0.3125^\circ$ resolution (Lucchesi, 2017). We use the nested model with a simulation domain of 19.25°N to 54.75°N and 61.5625°W to 130°W (domain of Fig. 1). Simulations are run for the full calendar year for each inversion year 2019-2024. Domain edges and initial conditions are defined by a globally archived set
 165 of TROPOMI smoothed boundary condition to ensure consistency with the observations used in the inversion (Estrada et al., 2025).

2.3 Prior estimates

Prior emission estimates for CONUS are summarized in Table 2. Anthropogenic emission estimates by sector are from the monthly GHGI at $0.1^\circ \times 0.1^\circ$ grid resolution (Maasakkers et al., 2023) produced annually from 2012 to 2020. 2020 GHGI
 170 values are used as prior estimates for subsequent years in the inversion. Prior estimates for a given year do not include information from posterior results for the previous year, as would be done in a Kalman filter, in order to apply consistent corrections to the bottom-up estimates from year to year. GHGI does not include emissions from hydroelectric reservoirs, which we add from the Reservoir Methane Emissions inventory (ResME; Delwiche et al., 2022) and account for 7% of anthropogenic emissions. Prior anthropogenic emission estimates for Mexico and Canada are from Scarpelli et al. (2020,
 175 2022), who spatially allocate the UNFCCC reports on a $0.1^\circ \times 0.1^\circ$ grid. Prior anthropogenic emission estimates for other



countries in the model domain are IMI defaults (Estrada et al., 2025). For wetlands, we use the 2019 mean estimate generated from the nine high-performance members of WetCHARTs v1.3.1 (Bloom et al., 2021) as prior estimate for all inversion years. Other minor natural sources include daily open fires from the Global Fire Emissions Database (GFED4) (Randerson et al., 2017), geological seeps (Hmiel et al., 2020), and termites (Fung et al., 1991).

180 **2.4 State vector clustering and sectoral attribution**

We apply the IMI's smart clustering algorithm (Estrada et al., 2025) to generate a multi-resolution state vector that aggregates native grid cells in areas with weak emissions and low observation density, while maintaining native $0.25^{\circ} \times 0.3125^{\circ}$ grid resolution in areas with strong emissions and high observation density. The same state vector clustering is used for all annual inversions and is based on the average observation density for 2019-2024 when applying the algorithm.

185 We force clusters to respect state boundaries to avoid aggregation error on the calculation of state total emissions.

The number of state vector elements defining the resolution of the inversion should maximize the DOFS while remaining computationally affordable. We determined the optimal number before running the inversion by estimating the DOFS for varying state vector sizes in the IMI preview as described by Estrada et al. (2025). We choose a state vector dimension of
190 2600 as this is where the gain in the DOFS plateaus. Additionally, we impose a maximum cluster size of 10 grid cells per element to maintain relatively high resolution across the domain.

The inversion returns posterior emissions on the $0.25^{\circ} \times 0.3125^{\circ}$ grid. Sectoral attribution is then done by applying the posterior/prior emission ratio in each grid cell to the prior sectoral emissions in that grid cell. This reliance on the
195 distribution of the prior emissions can lead to high uncertainty of sectoral disaggregation in regions where there is close collocation of emission sources. Using native grid resolution for the state vector in high-emission areas minimizes the sectoral attribution error resulting from spatial overlap between sectors. Spatially averaged posterior emissions (total and by sector) are obtained by applying a summation matrix (Nesser et al., 2024).

3 Results and discussion

200 **3.1 Evaluation of inversion results**

We evaluate our inversion results by comparing the GEOS-Chem simulation with posterior emissions (Fig. 1) to the TROPOMI observations used in the inversion and to independent observations from surface, aircraft, and tower observations in the NOAA CH₄ GLOBALVIEWplus v7.0 data product (Schuldt et al., 2024). Following Lu et al. (2022), NOAA observations are sampled during daytime hours (10:00-16:00 local time) and only include observations within 3 standard
205 deviations from the daily mean, or 2 standard deviations if the standard deviation is greater than 30 ppb. We compare the model to the annual ensemble mean observations for each site for 2019-2023. Figure 2 shows improvements in RMSE and



mean bias in the TROPOMI residuals relative to the prior estimate (panels a and b), a shift of the residual distribution toward zero (panel c), and a general whitening of noise across the domain, indicating improved agreement with the observations. Independent observations (panel d) show a 5.6 ppb improvement in mean bias relative to the prior estimate and a 5.3 ppb improvement in RMSE. The coefficient of determination (R^2) increases from 0.61 to 0.74.

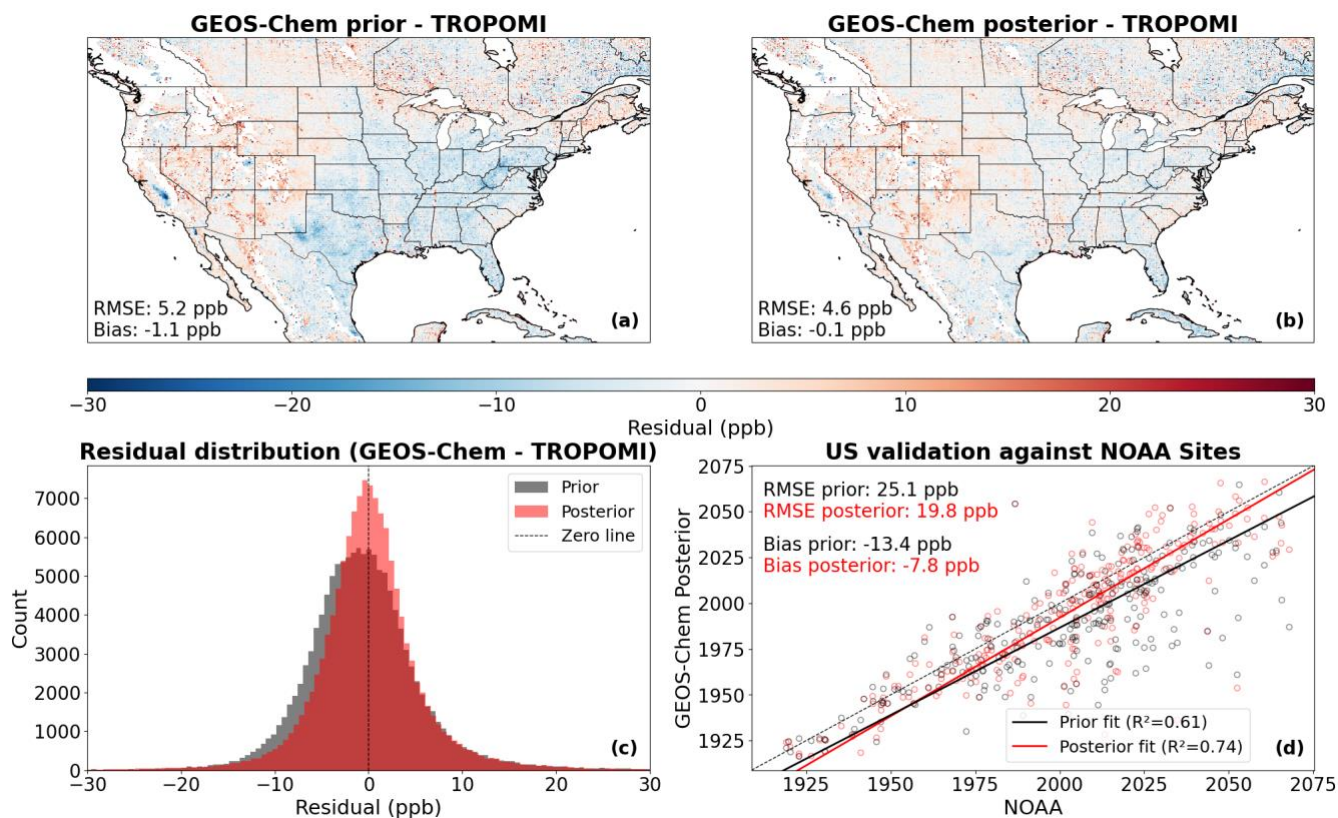


Figure 2: Evaluation of the prior and posterior emission estimates when implemented in the GEOS-Chem simulation. The top panels show the gridded annual mean residuals between GEOS-Chem and the TROPOMI observations for the (a) prior and (b) posterior simulations. Panel (c) shows the tightening of the residual distribution in the posterior estimate (red) versus the prior estimate (grey). Panel (d) shows comparison with independent NOAA site observations, where each point represents an annual afternoon mean. Root-mean-square errors (RMSE), mean biases, and reduced-major-axis regression lines are inset.

3.2 National emissions and trends, 2019-2024

Table 2 summarizes sector-resolved methane emissions for CONUS. Our mean posterior estimate of total methane emissions is 47 Tg a⁻¹ with 10 Tg a⁻¹ from natural sources and 37 Tg a⁻¹ from anthropogenic sources for the 2019-2024 period. This estimate is 34% higher than reported in the GHGI and 64% higher for oil/gas emissions. Livestock and landfills are adjusted upward by 29% and 30%, respectively. Our results are consistent with the large underestimates found in other studies (Turner et al., 2015; Maasackers et al., 2021; Lu et al., 2022; Worden et al., 2022; Lu et al., 2023; Nesser et al., 2024), which continue to exist in the most recent gridded GHGI. Results for individual sectors broadly agree with previous studies (Fig.



225 S1) regardless of differences in time period, satellite product, prior inventory, and inversion methodology. Results for hydroelectric reservoirs show little departure from the ResME inventory used as prior estimate. Posterior emission estimates for wetlands and other natural sources also show little departure from the prior estimates.

Table 2: Methane emissions in the contiguous U.S. (CONUS)

	GHGI (Tg a⁻¹)^a	This work (Tg a⁻¹)^b
Averaging Period	2017-2020	2019-2024
Anthropogenic Total	27.7	37.2 (31.7-44.7)
Livestock	9.4	12.1 (10.9-14.4)
Oil/gas	7.6	12.5 (10.3-15.0)
Gas	6.4	9.9 (8.3-11.9)
Oil	1.2	2.6 (2.0-3.1)
Coal	2.2	2.6 (2.3-3.0)
Landfills	4.4	5.7 (4.9-7.1)
Wastewater	0.7	0.9 (0.8-1.1)
Rice	0.5	0.5 (0.5-0.6)
Other^c	0.8	1.0 (0.9-1.2)
Hydroelectricity	2.0	1.8 (1.2-2.3)
Natural	9.5	9.9 (8.1-11.7)
Wetlands	8.2	8.5 (7.0-10.0)
Fires	0.4	0.4 (0.3-0.5)
Seeps	0.3	0.3 (0.2-0.3)
Termites	0.6	0.7 (0.6-0.9)

230 ^aMean of 2017-2020 U.S. EPA Greenhouse Gas Inventory (GHGI) for anthropogenic sources with hydroelectric reservoir emissions added (Delwiche et al., 2022).

^b Annual mean best posterior estimates over averaging period (2019-2024), with ranges from the inversion ensemble in parentheses.

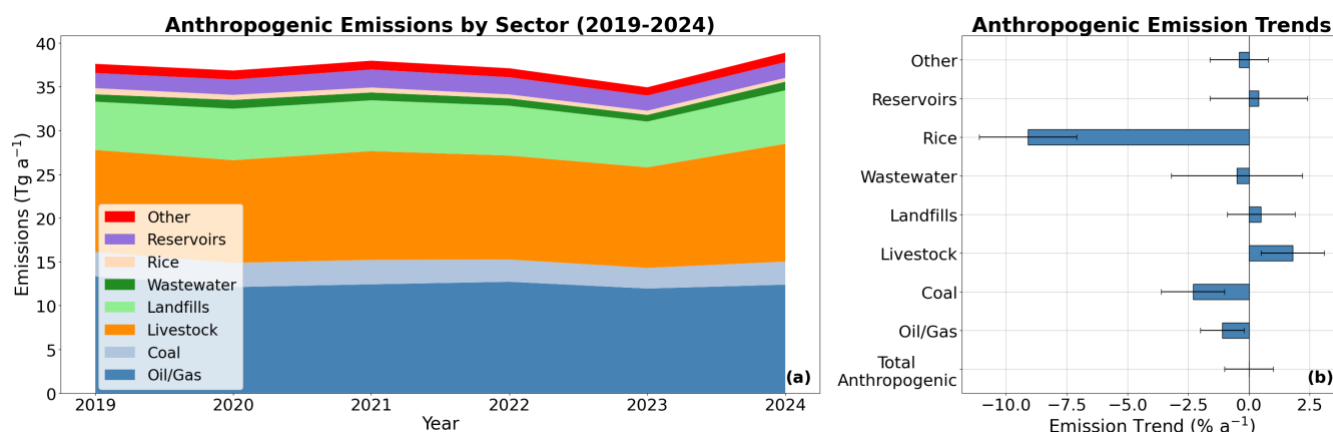
^c Fossil fuel combustion, industrial processes, agricultural burning, and composting.

235 Figure 3 shows our posterior emission estimates for each year and the sector-specific trends for 2019-2024. Trends are derived through Ordinary Least Squares (OLS) regression of the mean sectoral emissions for each year. Uncertainties are the corresponding standard error of estimates from the regression line. Total anthropogenic emissions are flat in our posterior estimate ($0.0 \pm 1.0\% \text{ a}^{-1}$), continuing the flat emissions trend of the 2017-2020 GHGI ($-0.5 \pm 0.6\% \text{ a}^{-1}$) and consistent with global inversions of TROPOMI data (He et al., 2025; Pendergrass et al., 2025). However, this overall flat trend reflects

240 offsetting trends from different sectors. Emissions from fuel exploitation declined over 2019-2024 by $-1.1 \pm 0.9\% \text{ a}^{-1}$ for oil/gas and $-2.3 \pm 1.3\% \text{ a}^{-1}$ for coal. The decrease of coal emissions continues the declining trends found in the 2017-2020



GHGI ($-8.7 \pm 1.2\% \text{ a}^{-1}$) and reflects reduced production from underground mines (Penn et al., 2026). Livestock emissions increase ($1.8 \pm 1.3\% \text{ a}^{-1}$), despite falling cattle populations (8% since 2019; USDA, 2025), suggesting that liquid manure systems may be responsible for the increase. This possible mechanism is supported by a rise in the number of Concentrated Animal Feeding Operations (CAFOs; NPDES CAFO Regulations Implementation Status Reports, 2025), which typically use liquid manure management systems. We do not find a significant trend in landfill emissions ($0.5 \pm 1.4\% \text{ a}^{-1}$), in contrast to a declining trend in the GHGI that Balasus et al. (2025) show to be an artifact from a switch in landfill emission models. For rice agriculture, we see a large decreasing trend ($-9.1 \pm 2.0\% \text{ a}^{-1}$), which may be due to increasing adoption of water-saving practices (Hardke et al., 2024).



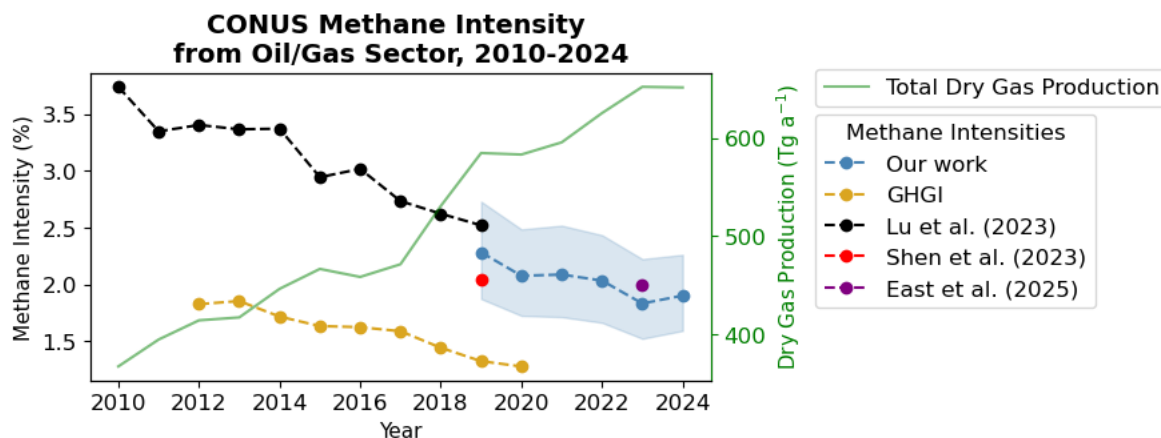
250

Figure 3: CONUS anthropogenic methane emissions and trends by sector, 2019-2024. Values are mean posterior estimates from our inversion ensemble. Trends are derived from ordinary least squares regression of emissions for individual years, and error bars are the standard error.

255

Methane intensity from the oil/gas sector is commonly defined as the total methane emissions along the oil/gas supply chain per unit of dry production of methane (Alvarez et al., 2018). We compute it using dry gas production data from the U.S. Energy Information Agency (EIA) assuming 85% methane content (EPA, 1998). We find decreasing methane intensity from 2.3% to 1.9% over the 2019-2024 period (Fig. 4). This continues the trend identified by Lu et al. (2023) for 2010-2019 and the consistent 2012-2020 trend in the GHGI. Our computed intensities are consistent with the 2019 values computed with GOSAT and NOAA observations (Lu et al., 2023) and with TROPOMI intensities for 2019 and 2023 (Shen et al., 2023; East et al., 2025). Others have found that declining intensities were due to increasing production with stable emissions, implying that emissions were decoupled from production (Lu et al., 2023; Varon et al., 2023). Here, we find that actual emissions decrease while production increases, demonstrating improvements in emission management.

260



265 Figure 4: National methane intensity trends for the oil/gas sector in CONUS, 2010-2024. The 2019-2024 trend from this work (best posterior estimate and range from the ensemble) is compared to a 2023 TROPOMI inversion (East et al., 2025), a 2019 inversion of older TROPOMI retrievals (Shen et al., 2023), the 2010-2019 trend from an inversion of GOSAT and NOAA observations (Lu et al., 2023), and the GHGI trend extending to 2020. Total dry gas production of methane is from the U.S. Energy and Information Administration (U.S. EIA, 2025).

270 3.3 Emissions and trends for individual states

Figure 5 shows anthropogenic emission totals and trends for individual U.S. states and Table 3 summarizes data for the top 10 emitting states, which together account for 55% of total anthropogenic U.S. emissions. Data for all states are in Table S1. Texas is the largest contributor, responsible for 19% of national anthropogenic emissions, primarily from oil/gas activity. Six of the top 10 states are dominated by oil/gas emissions, and all six show upward oil/gas adjustments relative to the GHGI:

275 Texas (+121%), Oklahoma (+100%), Pennsylvania (+47%), Ohio (+41%), New Mexico (+98%), and Louisiana (+69%). Texas, Oklahoma, and New Mexico exhibit particularly high oil/gas sector methane intensities (Fig. 5). In general, we find that states with dominant fossil fuel emissions show declining trends and states with dominant livestock emissions show increasing trends. Texas, California, and Nebraska are the largest livestock emitters, reflecting their large animal populations, but national trends are disproportionately influenced by livestock emissions increases in Iowa ($8.3 \pm 4.8 \% a^{-1}$),

280 Kansas ($7.0 \pm 2.1 \% a^{-1}$), and Missouri ($5.4 \pm 4.3 \% a^{-1}$). These increases cannot be explained by herd size, as livestock populations remained stable in Iowa, although with higher hog populations (USDA, 2025), and declined in Kansas and Missouri. Dairy cattle numbers rose in Iowa and Kansas but insufficiently to account for the observed emission trend. This combination suggests that manure management, which represents 26% of national livestock emissions (Maasackers et al., 2023), is driving the increase. Rice emissions are concentrated in Arkansas and Louisiana and drive the decline in Arkansas'

285 methane emissions, potentially driven by changing agricultural practices (Hardke et al., 2024) with methane reduction benefits (Runkle et al., 2019; Karki et al., 2021) and declining summer precipitation during 2019-2024 (NCEI, 2025).



290 Twenty-one states within CONUS produce their own greenhouse gas inventories, independent of the GHGI, using either custom-built frameworks or the EPA State Inventory Tool (SIT) with state-specific inputs (EPA, 2022). Here, we examine the available state inventories for the top ten emitting states, plus Colorado, and find that state-specific data do not always lead to improvements over the GHGI. Louisiana's inventory (Dismukes, 2021), based on the EPA SIT tool, is considerably lower than both the GHGI and our estimate, largely due to differences in reported oil/gas and landfill emissions. Pennsylvania is one of the highest producers of natural gas and has long shown very low methane intensity in the oil/gas sector, as seen in Fig. 5 and in other studies (Cardoso-Saldaña et al., 2021; Lu et al., 2023). The state inventory for Pennsylvania (Pennsylvania DEP, 2025) uses the EPA SIT but applies Appalachian-specific emission factors and incorporates more information on well type and counts from private data. It reports oil/gas emissions 30% higher than the GHGI, aligning with the range of uncertainty in our estimate. However, despite close agreement with our work for oil/gas, Pennsylvania inventory totals are slightly lower than the GHGI estimate due to very low reported landfill emissions, which are substantially lower than both the GHGI and our estimate. This discrepancy may arise from overestimated landfill gas recovery efficiencies used to calculate total emissions (Balasus et al., 2025; Wang et al., 2025).

305 In 2017, California adopted targets to reduce 75% of landfill emissions by 2025 relative to 2014 and 40% of manure management emissions by 2030 relative to 2013 (California Legislature, 2016), alongside comprehensive oil/gas regulations (CARB, 2017). The California Air Resources Board (CARB) generates annual emission estimates using custom methodology and state specific activity data to track state emission goals. California is the only state among the top 10 where our inversion adjusted emissions downward from the GHGI (-7%) with particularly large decreases for oil/gas (-20%) and landfills (-30%). Comparison with the CARB inventory (CARB, 2025) shows closer agreement across all sectors except oil/gas, reflecting the accuracy of non-fossil California data sources and reporting programs (Appuhamy and Kebreab, 2018). Comparisons of our results for individual sectors with the California inventory are shown in Fig. S2.

310 In 2021, New Mexico mandated a <2% methane intensity for oil/gas operations by 2026, frequent leak detection and repair (LDAR), and restrictions on flaring and venting beginning in 2021 (New Mexico Oil Conservation Commission, 2021). The state is home to a subset of the Permian basin, where high methane intensities have previously been documented (Zhang et al., 2020; Schneising et al., 2020; Liu et al., 2021; Y. Chen et al., 2022; Shen et al., 2022; Varon et al., 2023). The state's inventory (Bharadwaj et al., 2024), based on detailed equipment-level data, yields higher emissions than the GHGI (+10%) but remains below our estimate (26% higher than GHGI). We find a substantial decline in methane intensity from 4.3% in 2019 to 1.7% in 2024, indicating that New Mexico has already achieved its target of <2%, though most reductions occurred before the 2021 regulations. This finding is corroborated by Varon et al. (2025), who found an intensity decrease from 4.5% to 2.1% during 2019-2023 over the New Mexico portion of the Permian basin.

320



Colorado targets a 50% reduction in greenhouse gas emissions by 2030 relative to 2005 (Colorado General Assembly, 2019), supported by measures including quarterly and semiannual LDAR, a ban on routine flaring, and a 2029 phaseout of pneumatic devices (CDPHE, 2025). We find downward adjustments for Colorado relative to the GHGI across all sectors except oil/gas, including livestock (-17%), landfills (-23%), and coal (-52%). The oil/gas sector is 12% higher than the GHGI estimate and corresponds to a mean oil/gas methane intensity of 1.1%. The Colorado Department of Public Health and Environment inventory (CDPHE; Twyman et al., 2024) is double the GHGI due to large overestimates in oil/gas emissions (+244%). This discrepancy, previously documented by Nesser et al. (2024), is likely attributable to the CDPHE’s assumption of high and outdated leakage rates (>2%).

330 **Table 3: Emissions and trends for the top ten emitting U.S. states^a**

State	GHGI (Tg a ⁻¹)	This work ^b (Tg a ⁻¹)	State Inventory (Tg a ⁻¹)	GHGI Trend ^c (% a ⁻¹)	Posterior Trend ^d (% a ⁻¹)	Highest sector ^e
Period	2017-2020	2019-2024	see footnotes	2017-2020	2019-2024	2019-2024
Texas	3.80	7.2 (5.8-8.6)	-	0.2 ± 0.8	-2.6 ± 1.3	Oil/Gas
Oklahoma	1.24	2.2 (1.8-2.7)	-	-0.4 ± 0.4	-1.4 ± 1.0	Oil/Gas
West Virginia	0.87	1.8 (1.5-2.1)	-	-6.0 ± 0.3	-0.7 ± 2.9	Coal
Pennsylvania	1.30	1.6 (1.3-2.0)	1.28 ^f	-3.2 ± 0.9	1.0 ± 2.3	Oil/Gas
California	1.64	1.5 (1.1-1.9)	1.47 ^g	-0.3 ± 0.1	1.6 ± 2.4	Livestock
Ohio	0.81	1.4 (1.1-1.6)	-	-2.2 ± 2.2	-1.8 ± 4.3	Oil/Gas
Kansas	0.94	1.3 (1.1-1.5)	-	1.6 ± 1.0	6.6 ± 2.2	Livestock
New Mexico	0.74	1.3 (1.0-1.5)	0.76 ^h	-0.1 ± 1.1	0.8 ± 4.2	Oil/Gas
Louisiana	0.80	1.2 (1.0-1.5)	0.37 ⁱ	-0.2 ± 1.8	-11.0 ± 2.3	Oil/Gas
Illinois	0.60	1.0 (0.8-1.3)	-	1.0 ± 0.6	-0.1 ± 5.9	Landfills
Colorado (#23)	0.71	0.6 (0.5-0.7)	1.43 ^j	-3.0 ± 0.2	2.0 ± 6.0	Oil/Gas

^a Mean emissions and linear regression trends ± standard error for the reported periods, for the top ten emitting states in our posterior estimate plus Colorado (discussed in the text).

^b Mean posterior estimate from our inversion, with uncertainty bounds in parentheses from the range of the inversion ensemble.

^c From a linear regression of GHGI estimates.

335 ^d From a linear regression of the mean of the inversion ensemble for individual years.

^e As determined by the posterior emissions estimate.

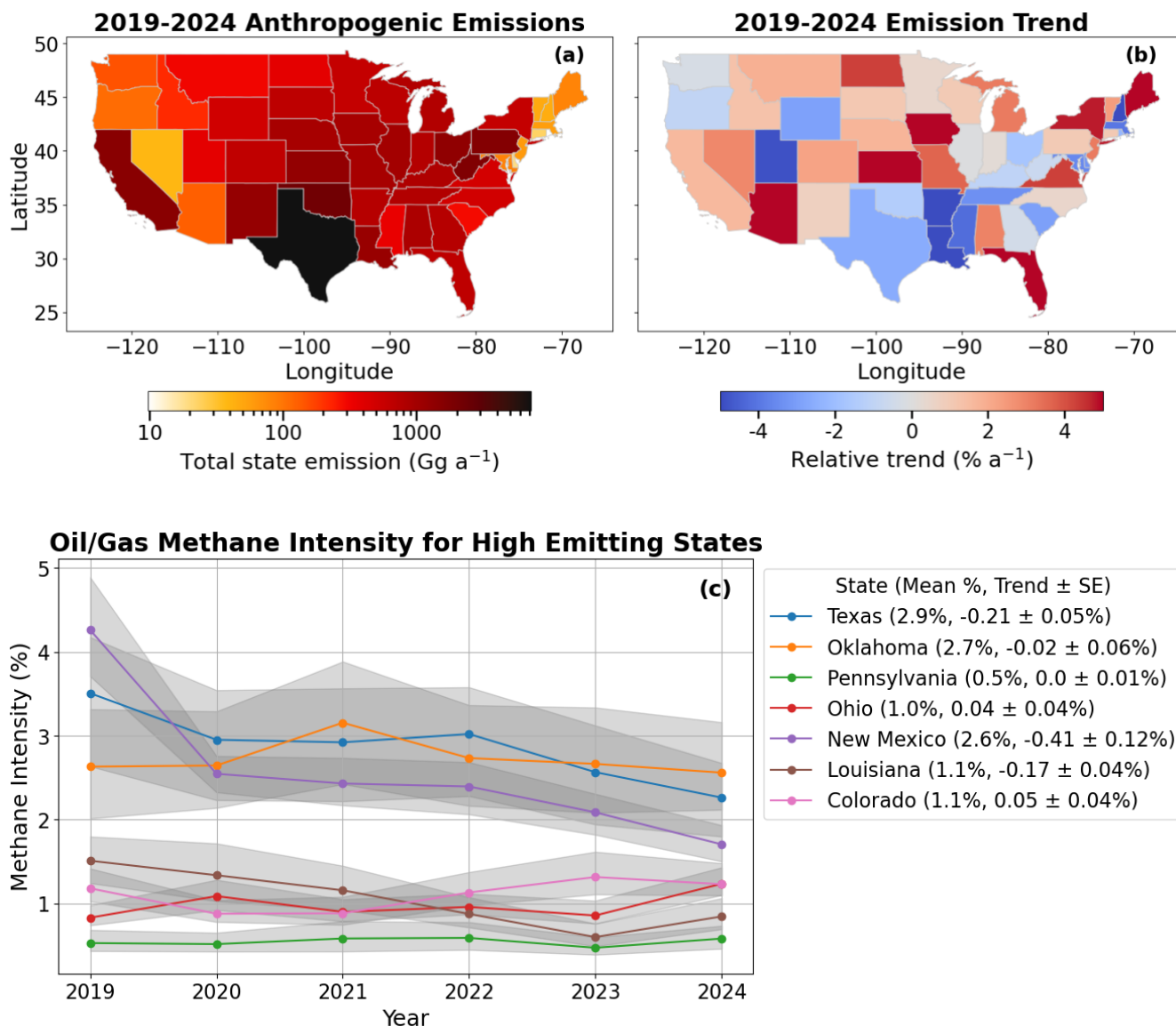
^f 2019-2022 (Pennsylvania DEP, 2025).

^g 2019-2023 (CARB, 2025).

^h 2021 (Bharadwaj et al., 2024).

340 ⁱ 2018 (Dismukes, 2021).

^j 2017-2020 (Twyman et al., 2024).



345 Figure 5: Mean 2019-2024 anthropogenic emissions, trends, and intensities for individual states. Panel (a) shows mean anthropogenic emissions on a log scale. Panel (b) shows the percent change per year from a linear regression of the emissions for each state. Panel (c) shows methane intensities from the oil/gas sector for the six states dominated by oil/gas emissions and Colorado. The trends and standard errors (SE) are from ordinary least squares regression of the mean intensity for each year. EIA data on individual state dry production for 2024 was unavailable at the time of writing, so we estimate dry production from marketed gas using the ratio of dry production to marketed gas in 2023.

350

3.4 Emissions and trends for oil/gas production fields

Figure 6 summarizes the oil/gas emissions and trends for the top 8 emitting oil/gas fields in CONUS. The Permian and Appalachian fields represent, respectively, 21% and 14% of CONUS oil/gas sector emissions with mean emissions of 2700

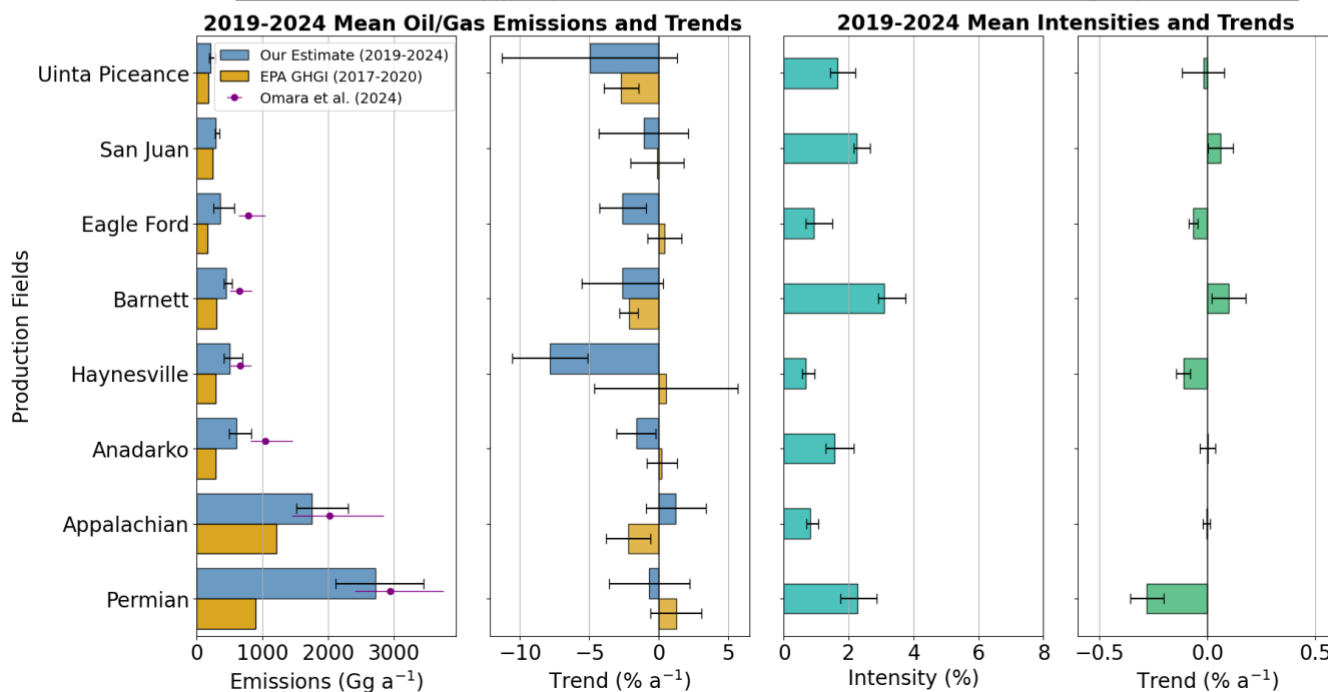
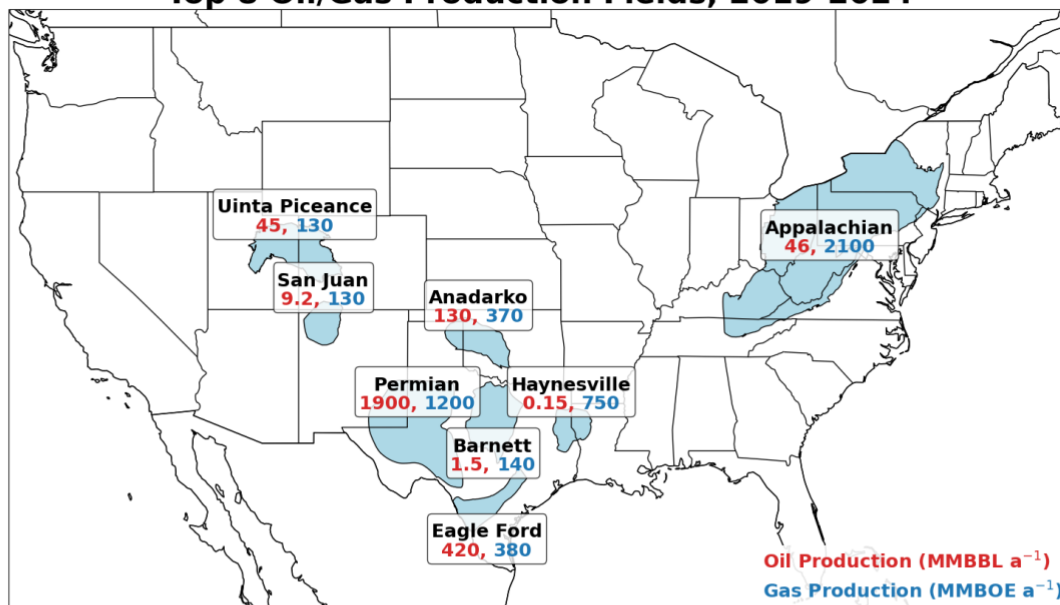


(2100-3400) Gg a⁻¹ and 1700 (1500-2300) Gg a⁻¹. Although the Appalachian's methane intensity is relatively low, its high
355 production volume makes it one of the highest total emitters among U.S. oil/gas fields. The Permian estimate is in the same
range as other top-down estimates from Shen et al. (2022), Varon et al. (2023), Lu et al. (2023), and Omara et al. (2024). We
find an average underestimate in the GHGI of 83% across the top 8 oil/gas production fields with the largest adjustment in
the Permian (+202%) and the lowest adjustment to the Uinta Piceance (+28%). We calculate methane intensities with the
integrated emissions from the oil/gas supply chain, but upstream emissions from production are the dominant source in the
360 top 8 oil/gas basins, so that methane intensity changes little if midstream or downstream emissions are excluded (Fig. S3).
We find particularly high methane intensities in the Barnett (3.1%), Permian (2.3%), and San Juan (2.2%). Oil-dominant
fields, like the Permian, may exhibit high methane intensities due to insufficient gathering and processing equipment for
capturing associated gas from oil production (Lu et al., 2023; Omara et al., 2024; Varon et al., 2025). The Barnett and San
Juan are gas-dominant fields that share common features: development peaked over a decade ago, production has since
365 declined, and new investment has been limited. In contrast, gas-dominant fields with active development have some of the
lowest intensities, including Haynesville (0.7%), Appalachian (0.8%), Anadarko (1.6%), and Uinta-Piceance (1.7%). The
oil-dominant Eagle Ford, which also has low methane intensity (0.9%), has rising gas production (and declining oil
production) during the study period, suggesting increased investment in gas infrastructure.

370 All high-emitting production fields experience declining (Anadarko, Haynesville, and Eagle Ford) or flat emissions trends,
consistent with findings for Texas oil/gas fields reported by Varon et al. (2025). The Haynesville and Eagle Ford fields
increased production while reducing emissions, demonstrating improvements in emissions management. The San Juan and
Barnett are the only fields in the top 8 with rising methane intensity. Their trends may reflect fixed emissions from aging
infrastructure comprising a growing share of total emissions as gas production decreases.



Top 8 Oil/Gas Production Fields, 2019-2024



375

Figure 6: 2019-2024 mean oil/gas production, emissions, emission intensities, and trends for the top eight oil/gas production fields in CONUS. Emissions and emission intensities are from the mean of our posterior estimates, with error bars representing the ranges from the inversion ensemble (for the 2019-2024 mean panels) or the standard error on the regression slopes (for the trends). Emission estimates from Omara et al. (2024) are for 2021 emissions. Trends are calculated using OLS regression on results for individual years. Production data were derived from the Enverus prism platform (Enverus, 2025). MMBBL is million barrels of oil and MMBOE is million barrels of oil equivalent. Oil/gas field boundaries are based on definitions in Omara et al. (2024).

380



4 Conclusions

We presented high-resolution annual methane emission estimates for the contiguous U.S. (CONUS) from 2019 to 2024 using
385 the open-source Integrated Methane Inversion (IMI 2.1) with TROPOMI satellite observations. The inversions used the EPA
Greenhouse Gas Inventory (GHGI) as prior estimate. Our goal is to support the GHGI going forward with an inversion
framework configured for consistent and transparent annual updates of U.S. methane emissions. Annual results are
visualized on a custom dashboard (laestrada.github.io/conus_emissions_viz/). Leveraging its open-source code, the system
has been ported to the NASA Multi-Mission Algorithm and Analysis Platform as part of the U.S. Greenhouse Gas Center
390 (U.S. GHG Center, 2025), demonstrating potential for annual updates and use by government and private stakeholders. It is
also available on the Amazon Web Services (AWS) cloud.

We find that mean CONUS anthropogenic emissions for 2019-2024 are 37 Tg a^{-1} , 34% above the GHGI, with oil/gas
emissions 64% above the GHGI. We find no significant 2019-2024 trend in CONUS emissions, but this result reflects
395 offsetting decreasing trends from oil/gas ($-1.1 \pm 0.9\% \text{ a}^{-1}$), coal ($-2.3 \pm 1.3\% \text{ a}^{-1}$) and rice ($-9.1 \pm 2.0\% \text{ a}^{-1}$) emissions and
increasing trends of livestock ($+1.8 \pm 1.3\% \text{ a}^{-1}$) and landfill ($+0.5 \pm 1.4\% \text{ a}^{-1}$) emissions. The signs of sectoral trends broadly
agree with the latest GHGI trends reported for 2017-2020 (except rice). National oil/gas methane intensity declined from
2.3% to 1.9% over the 2019-2024 period, continuing a previously reported declining trend for 2010-2019 and consistent with
the GHGI. Unlike the 2010-2019 trend, however, we find that emissions themselves have declined, demonstrating improved
400 management to reduce emissions.

We find that over half of U.S. anthropogenic methane is emitted from just ten states. Texas alone contributes 18%. Texas
and other oil/gas-dominated states (Oklahoma, New Mexico, Ohio, Louisiana) show declining or flat trends over 2019-2024.
New Mexico's oil/gas intensity fell from 4.3% in 2019 to 1.7% in 2024, effectively meeting the state's <2% target for
405 methane intensity from the oil/gas sector. Kansas and Iowa show significant 2019-2024 increases in emissions driven by
livestock. Arkansas shows decreasing emissions driven by rice agriculture. Emission inventories constructed by individual
states using state-specific data do not always improve upon GHGI estimates. Colorado, for instance, considerably
overestimates its oil/gas emissions, likely because it uses obsolete emission factors.

Most major U.S. oil/gas production fields show stable or declining emissions. The Haynesville and Eagle Ford show rising
410 production with falling emissions, exhibiting field-level evidence of improved capture rates. Rising methane intensities are
driven by declining production, suggesting a dominance of aging or abandoned infrastructure. Gas-dominant fields generally
exhibit lower intensities, though the low-intensity Appalachian basin now ranks as a top-emitting field due to its high level
of gas production. This work highlights how sustained satellite-based inversions can identify trends and discrepancies across
415 sectors and play an increasingly critical role in U.S. methane emissions monitoring going forward.



Acknowledgments

This research was supported in part at the Jet Propulsion Laboratory, California Institute of Technology, under a contract with the National Aeronautics and Space Administration (80NM0018D0004) for the US Greenhouse Gas Center, the Harvard Methane Initiative, the NASA Carbon Monitoring System, and ExxonMobil Technology and Engineering Company.

Data Availability

The IMI source code and documentation is available at <https://carboninversion.com/>. The blended TROPOMI+GOSAT satellite observations are available at <https://registry.opendata.aws/blended-tropomi-gosat-methane> (Balasus et al., 2023). Visualized results dashboard available at https://laestrada.github.io/conus_emissions_viz/. The emissions estimates, configuration, and analysis code are available at https://github.com/laestrada/CONUS_project_imi/. GEOS-Chem chemical transport model code is available at <https://doi.org/10.5281/zenodo.12584192>.

Author Contributions

LAE, DJJ, and KWB designed the study. LAE conducted the inversions and analysis with contributions from DJJ, MS, MH, JDE, and DJV. LAE and DJJ wrote the paper with input from all authors.

References

- Alvarez, R. A., Zavala-Araiza, D., Lyon, D. R., Allen, D. T., Barkley, Z. R., Brandt, A. R., Davis, K. J., Herndon, S. C., Jacob, D. J., Karion, A., Kort, E. A., Lamb, B. K., Lauvaux, T., Maasakkers, J. D., Marchese, A. J., Omara, M., Pacala, S. W., Peischl, J., Robinson, A. L., Shepson, P. B., Sweeney, C., Townsend-Small, A., Wofsy, S. C., and Hamburg, S. P.: Assessment of methane emissions from the U.S. oil and gas supply chain, *Science*, 361, 186–188, <https://doi.org/10.1126/science.aar7204>, 2018.
- Appuhamy, R. and Kebreab, E.: Characterizing California-specific Cattle Feed Rations and Improve Modeling of Enteric Fermentation for California’s Greenhouse Gas Inventory, California Environmental Protection Agency, Air Resources Board, Research Division, 52 pp., 2018.
- Balasus, N., Jacob, D. J., Lorente, A., Maasakkers, J. D., Parker, R. J., Boesch, H., Chen, Z., Kelp, M. M., Nesser, H., and Varon, D. J.: A blended TROPOMI+GOSAT satellite data product for atmospheric methane using machine learning to correct retrieval biases, *Atmos. Meas. Tech.*, 16, 3787–3807, <https://doi.org/10.5194/amt-16-3787-2023>, 2023.
- Balasus, N., Jacob, D. J., Maxemin, G., Jenks, C., Nesser, H., Maasakkers, J. D., Cusworth, D. H., Scarpelli, T. R., Varon, D. J., and Wang, X.: Satellite monitoring of annual US landfill methane emissions and trends, *Environ. Res. Lett.*, 20, 024007, <https://doi.org/10.1088/1748-9326/ada2b1>, 2025.
- Barré, J., Aben, I., Agustí-Panareda, A., Balsamo, G., Bousserez, N., Dueben, P., Engelen, R., Inness, A., Lorente, A., McNorton, J., Peuch, V.-H., Radnoti, G., and Ribas, R.: Systematic detection of local CH₄ anomalies by combining satellite measurements with high-resolution forecasts, *Atmospheric Chemistry and Physics*, 21, 5117–5136, <https://doi.org/10.5194/acp-21-5117-2021>, 2021.



- 455 Bharadwaj, S., Clark, T., Loken, R., and Trivedi, D.: New Mexico Greenhouse Gas Emissions Inventory and Forecast, 2024.
- Bloom, A. A., Bowman, K. W., Lee, M., Turner, A. J., Schroeder, R., Worden, J. R., Weidner, R. J., McDonald, K. C., and Jacob, D. J.: CMS: Global 0.5-deg Wetland Methane Emissions and Uncertainty (WetCHARTs v1.3.1), ORNL DAAC, <https://doi.org/10.3334/ORNLDAAC/1915>, 2021.
- 460 Brasseur, G. P. and Jacob, D. J.: Modeling of Atmospheric Chemistry, Cambridge University Press, Cambridge, <https://doi.org/10.1017/9781316544754>, 2017.
- Bruhwyler, L. M., Basu, S., Bergamaschi, P., Bousquet, P., Dlugokencky, E., Houweling, S., Ishizawa, M., Kim, H.-S., Locatelli, R., Maksyutov, S., Montzka, S., Pandey, S., Patra, P. K., Petron, G., Saunio, M., Sweeney, C., Schwietzke, S., 465 Tans, P., and Weatherhead, E. C.: U.S. CH₄ emissions from oil and gas production: Have recent large increases been detected?, *Journal of Geophysical Research: Atmospheres*, 122, 4070–4083, <https://doi.org/10.1002/2016JD026157>, 2017.
- Buchwitz, M., Schneising, O., Reuter, M., Heymann, J., Krautwurst, S., Bovensmann, H., Burrows, J. P., Boesch, H., Parker, R. J., Somkuti, P., Detmers, R. G., Hasekamp, O. P., Aben, I., Butz, A., Frankenberg, C., and Turner, A. J.: Satellite-derived 470 methane hotspot emission estimates using a fast data-driven method, *Atmospheric Chemistry and Physics*, 17, 5751–5774, <https://doi.org/10.5194/acp-17-5751-2017>, 2017.
- California Air Resources Board: Greenhouse Gas Emission Standards for Crude Oil and Natural Gas Facilities, California Code of Regulations, Title 17, Div. 3, Ch. 1, Subch. 10, Art. 4, Subart. 13, 2017.
- 475 California Legislature: Senate Bill 1383 (Short-Lived Climate Pollutant Reduction Law), California Health and Safety Code, § 39730.5 et seq., 2016.
- CARB: California Greenhouse Gas Emissions from 2000 to 2023: Trends of Emissions and Other Indicators, California Air 480 Resources Board, 2025.
- Cardoso-Saldaña, F. J. and Allen, D. T.: Projecting the Temporal Evolution of Methane Emissions from Oil and Gas Production Basins, *Environ. Sci. Technol.*, 55, 2811–2819, <https://doi.org/10.1021/acs.est.0c04224>, 2021.
- 485 Chen, Y., Sherwin, E. D., Berman, E. S. F., Jones, B. B., Gordon, M. P., Wetherley, E. B., Kort, E. A., and Brandt, A. R.: Quantifying Regional Methane Emissions in the New Mexico Permian Basin with a Comprehensive Aerial Survey, *Environ. Sci. Technol.*, 56, 4317–4323, <https://doi.org/10.1021/acs.est.1c06458>, 2022.
- 490 Chen, Z., Jacob, D. J., Nesser, H., Sulprizio, M. P., Lorente, A., Varon, D. J., Lu, X., Shen, L., Qu, Z., Penn, E., and Yu, X.: Methane emissions from China: a high-resolution inversion of TROPOMI satellite observations, *Atmospheric Chemistry and Physics*, 22, 10809–10826, <https://doi.org/10.5194/acp-22-10809-2022>, 2022.
- Chen, Z., Jacob, D. J., Gautam, R., Omara, M., Stavins, R. N., Stowe, R. C., Nesser, H., Sulprizio, M. P., Lorente, A., Varon, 495 D. J., Lu, X., Shen, L., Qu, Z., Pendergrass, D. C., and Hancock, S.: Satellite quantification of methane emissions and oil–gas methane intensities from individual countries in the Middle East and North Africa: implications for climate action, *Atmospheric Chemistry and Physics*, 23, 5945–5967, <https://doi.org/10.5194/acp-23-5945-2023>, 2023.
- Colorado Department of Public Health and Environment: Regulation Number 7: Control of Emissions from Oil and Gas 500 Operations, Code of Colorado Regulations, 5 CCR 1001-9, 2025.



Colorado General Assembly: Climate Action Plan to Reduce Pollution Act, Colorado Revised Statutes, C.R.S. § 25-7-102 and related provisions, 2019.

- 505 Crippa, M., Guizzardi, D., Pagani, F., Schiavina, M., Melchiorri, M., Pisoni, E., Graziosi, F., Muntean, M., Maes, J., Dijkstra, L., Van Damme, M., Clarisse, L., and Coheur, P.: Insights into the spatial distribution of global, national, and subnational greenhouse gas emissions in the Emissions Database for Global Atmospheric Research (EDGAR v8.0), *Earth System Science Data*, 16, 2811–2830, <https://doi.org/10.5194/essd-16-2811-2024>, 2024.
- 510 Cui, Y. Y., Henze, D. K., Brioude, J., Angevine, W. M., Liu, Z., Bousserez, N., Guerrette, J., McKeen, S. A., Peischl, J., Yuan, B., Ryerson, T., Frost, G., and Trainer, M.: Inversion Estimates of Lognormally Distributed Methane Emission Rates From the Haynesville-Bossier Oil and Gas Production Region Using Airborne Measurements, *Journal of Geophysical Research: Atmospheres*, 124, 3520–3531, <https://doi.org/10.1029/2018JD029489>, 2019.
- 515 Delwiche, K. B., Harrison, J. A., Maasackers, J. D., Sulprizio, M. P., Worden, J., Jacob, D. J., and Sunderland, E. M.: Estimating Drivers and Pathways for Hydroelectric Reservoir Methane Emissions Using a New Mechanistic Model, *Journal of Geophysical Research: Biogeosciences*, 127, e2022JG006908, <https://doi.org/10.1029/2022JG006908>, 2022.
- 520 Dismukes, D. E.: Louisiana 2021 Greenhouse Gas Inventory, https://www.lsu.edu/ces/publications/2021/louisiana-2021-greenhouse-gas-inventory-df-rev_reduced.pdf, 2021.
- Enverus PRISM platform: <https://prism.enverus.com/prism/home>, last access: 5 September 2025.
- EPA: AP-42: Compilation of Air Emissions Factors from Stationary Sources, 1998.
- 525 NPDES CAFO Regulations Implementation Status Reports: <https://www.epa.gov/npdes/npdes-cafo-regulations-implementation-status-reports>, last access: 18 November 2025.
- 530 East, J. D., Jacob, D. J., Jervis, D., Balasus, N., Estrada, L. A., Hancock, S. E., Sulprizio, M. P., Thomas, J., Wang, X., Chen, Z., Varon, D. J., and Worden, J. R.: Worldwide inference of national methane emissions by inversion of satellite observations with UNFCCC prior estimates, *Nat Commun*, 16, 11004, <https://doi.org/10.1038/s41467-025-67122-8>, 2025.
- EPA, EPA Inventory of U.S. Greenhouse Gas Emissions and Sinks: 1990-2022, EPA 430-R-24-004. <https://www.epa.gov/ghgemissions/inventory-us-greenhouse-gas-emissions-and-sinks-1990-2022>, 2024.
- 535 EPA: Learn more about Official State Greenhouse Gas Inventories: <https://www.epa.gov/ghgemissions/learn-more-about-official-state-greenhouse-gas-inventories>, last access: 21 November 2025.
- 540 Eskes, H. J., Velthoven, P. F. J. V., Valks, P. J. M., and Kelder, H. M.: Assimilation of GOME total-ozone satellite observations in a three-dimensional tracer-transport model, *Quarterly Journal of the Royal Meteorological Society*, 129, 1663–1681, <https://doi.org/10.1256/qj.02.14>, 2003.
- 545 Estrada, L. A., Varon, D. J., Sulprizio, M., Nesser, H., Chen, Z., Balasus, N., Hancock, S. E., He, M., East, J. D., Mooring, T. A., Oort Alonso, A., Maasackers, J. D., Aben, I., Baray, S., Bowman, K. W., Worden, J. R., Cardoso-Saldaña, F. J., Reidy, E., and Jacob, D. J.: Integrated Methane Inversion (IMI) 2.0: an improved research and stakeholder tool for monitoring total methane emissions with high resolution worldwide using TROPOMI satellite observations, *Geoscientific Model Development*, 18, 3311–3330, <https://doi.org/10.5194/gmd-18-3311-2025>, 2025.
- 550 Fung, I., John, J., Lerner, J., Matthews, E., Prather, M., Steele, L. P., and Fraser, P. J.: Three-dimensional model synthesis of the global methane cycle, *Journal of Geophysical Research: Atmospheres*, 96, 13033–13065, <https://doi.org/10.1029/91JD01247>, 1991.



- Forster, P., Storelvmo, T., Armour, K., Collins, W., Dufresne, J.-L., Frame, D., Lunt, D. J., Mauritsen, T., Palmer, M. D., Watanabe, M., Wild, M., and Zhang, H.: The Earth's Energy Budget, Climate Feedbacks and Climate Sensitivity, in: 555 Climate Change 2021 – The Physical Science Basis: Working Group I Contribution to the Sixth Assessment Report of the Intergovernmental Panel on Climate Change, Cambridge University Press, 923–1054, 2021.
- Hancock, S. E., Jacob, D. J., Chen, Z., Nesser, H., Davitt, A., Varon, D. J., Sulprizio, M. P., Balasus, N., Estrada, L. A., Cazorla, M., Dawidowski, L., Diez, S., East, J. D., Penn, E., Randles, C. A., Worden, J., Aben, I., Parker, R. J., and 560 Maasackers, J. D.: Satellite quantification of methane emissions from South American countries: a high-resolution inversion of TROPOMI and GOSAT observations, *Atmospheric Chemistry and Physics*, 25, 797–817, <https://doi.org/10.5194/acp-25-797-2025>, 2025.
- Hardke, J., Sha, X., and Bateman, N.: B.R. Wells Arkansas Rice Research Studies 2021, Arkansas Agricultural Experiment 565 Station Research Series, 9–17, 2024.
- He, M., Jacob, D. J., Estrada, L. A., Varon, D. J., Sulprizio, M., Balasus, N., East, J. D., Penn, E., Pendergrass, D. C., Chen, Z., Mooring, T. A., Maasackers, J. D., Brodrick, P. G., Frankenberg, C., Bowman, K. W., and Bruhwiler, L.: Attributing 570 2019–2024 methane growth using TROPOMI satellite observations, n.d.
- Hmiel, B., Petrenko, V. V., Dyonisius, M. N., Buizert, C., Smith, A. M., Place, P. F., Harth, C., Beaudette, R., Hua, Q., Yang, B., Vimont, I., Michel, S. E., Severinghaus, J. P., Etheridge, D., Bromley, T., Schmitt, J., Faïn, X., Weiss, R. F., and Dlugokencky, E.: Preindustrial 14CH₄ indicates greater anthropogenic fossil CH₄ emissions, *Nature*, 578, 409–412, 575 <https://doi.org/10.1038/s41586-020-1991-8>, 2020.
- Houweling, S., Bergamaschi, P., Chevallier, F., Heimann, M., Kaminski, T., Krol, M., Michalak, A. M., and Patra, P.: Global inverse modeling of CH₄ sources and sinks: an overview of methods, *Atmospheric Chemistry and Physics*, 17, 235–256, <https://doi.org/10.5194/acp-17-235-2017>, 2017.
- 580 Jacob, D. J., Turner, A. J., Maasackers, J. D., Sheng, J., Sun, K., Liu, X., Chance, K., Aben, I., McKeever, J., and Frankenberg, C.: Satellite observations of atmospheric methane and their value for quantifying methane emissions, *Atmospheric Chemistry and Physics*, 16, 14371–14396, <https://doi.org/10.5194/acp-16-14371-2016>, 2016.
- Jacob, D. J., Varon, D. J., Cusworth, D. H., Dennison, P. E., Frankenberg, C., Gautam, R., Guanter, L., Kelley, J., 585 McKeever, J., Ott, L. E., Poulter, B., Qu, Z., Thorpe, A. K., Worden, J. R., and Duren, R. M.: Quantifying methane emissions from the global scale down to point sources using satellite observations of atmospheric methane, *Atmospheric Chemistry and Physics*, 22, 9617–9646, <https://doi.org/10.5194/acp-22-9617-2022>, 2022.
- Karion, A., Sweeney, C., Pétron, G., Frost, G., Michael Haresty, R., Kofler, J., Miller, B. R., Newberger, T., Wolter, S., 590 Banta, R., Brewer, A., Dlugokencky, E., Lang, P., Montzka, S. A., Schnell, R., Tans, P., Trainer, M., Zamora, R., and Conley, S.: Methane emissions estimate from airborne measurements over a western United States natural gas field, *Geophysical Research Letters*, 40, 4393–4397, <https://doi.org/10.1002/grl.50811>, 2013.
- Karki, S., Adviento-Borbe, M. A. A., Massey, J. H., and Reba, M. L.: Assessing Seasonal Methane and Nitrous Oxide 595 Emissions from Furrow-Irrigated Rice with Cover Crops, *Agriculture*, 11, 261, <https://doi.org/10.3390/agriculture11030261>, 2021.
- Kort, E. A., Eluszkiewicz, J., Stephens, B. B., Miller, J. B., Gerbig, C., Nehrkorn, T., Daube, B. C., Kaplan, J. O., Houweling, S., and Wofsy, S. C.: Emissions of CH₄ and N₂O over the United States and Canada based on a receptor-oriented modeling framework and COBRA-NA atmospheric observations, *Geophysical Research Letters*, 35, 600 <https://doi.org/10.1029/2008GL034031>, 2008.



- 605 Kort, E. A., Frankenberg, C., Costigan, K. R., Lindenmaier, R., Dubey, M. K., and Wunch, D.: Four corners: The largest US methane anomaly viewed from space, *Geophysical Research Letters*, 41, 6898–6903, <https://doi.org/10.1002/2014GL061503>, 2014.
- 610 Lan, X., Tans, P., Sweeney, C., Andrews, A., Dlugokencky, E., Schwietzke, S., Kofler, J., McKain, K., Thoning, K., Crotwell, M., Montzka, S., Miller, B. R., and Biraud, S. C.: Long-Term Measurements Show Little Evidence for Large Increases in Total U.S. Methane Emissions Over the Past Decade, *Geophysical Research Letters*, 46, 4991–4999, <https://doi.org/10.1029/2018GL081731>, 2019.
- 615 Liu, M., van der A, R., van Weele, M., Eskes, H., Lu, X., Veeffkind, P., de Laat, J., Kong, H., Wang, J., Sun, J., Ding, J., Zhao, Y., and Weng, H.: A New Divergence Method to Quantify Methane Emissions Using Observations of Sentinel-5P TROPOMI, *Geophysical Research Letters*, 48, e2021GL094151, <https://doi.org/10.1029/2021GL094151>, 2021.
- 620 Lorente, A., Borsdorff, T., Butz, A., Hasekamp, O., aan de Brugh, J., Schneider, A., Wu, L., Hase, F., Kivi, R., Wunch, D., Pollard, D. F., Shiomi, K., Deutscher, N. M., Velasco, V. A., Roehl, C. M., Wennberg, P. O., Warneke, T., and Landgraf, J.: Methane retrieved from TROPOMI: improvement of the data product and validation of the first 2 years of measurements, *Atmospheric Measurement Techniques*, 14, 665–684, <https://doi.org/10.5194/amt-14-665-2021>, 2021.
- 625 Lu, X., Jacob, D. J., Wang, H., Maasackers, J. D., Zhang, Y., Scarpelli, T. R., Shen, L., Qu, Z., Sulprizio, M. P., Nesser, H., Bloom, A. A., Ma, S., Worden, J. R., Fan, S., Parker, R. J., Boesch, H., Gautam, R., Gordon, D., Moran, M. D., Reuland, F., Villasana, C. A. O., and Andrews, A.: Methane emissions in the United States, Canada, and Mexico: evaluation of national methane emission inventories and 2010–2017 sectoral trends by inverse analysis of in situ (GLOBALVIEWplus CH4 ObsPack) and satellite (GOSAT) atmospheric observations, *Atmospheric Chemistry and Physics*, 22, 395–418, <https://doi.org/10.5194/acp-22-395-2022>, 2022.
- 630 Lu, X., Jacob, D. J., Zhang, Y., Shen, L., Sulprizio, M. P., Maasackers, J. D., Varon, D. J., Qu, Z., Chen, Z., Hmiel, B., Parker, R. J., Boesch, H., Wang, H., He, C., and Fan, S.: Observation-derived 2010–2019 trends in methane emissions and intensities from US oil and gas fields tied to activity metrics, *Proceedings of the National Academy of Sciences*, 120, e2217900120, <https://doi.org/10.1073/pnas.2217900120>, 2023.
- 635 Lucchesi, R., 2017: File Specification for GEOS-5 FP. GMAO Office Note No. 4 (Version 1.1), 61 pp, available from http://gmao.gsfc.nasa.gov/pubs/office_notes.
- 640 Maasackers, J. D., Jacob, D. J., Sulprizio, M. P., Turner, A. J., Weitz, M., Wirth, T., Hight, C., DeFigueiredo, M., Desai, M., Schmeltz, R., Hockstad, L., Bloom, A. A., Bowman, K. W., Jeong, S., and Fischer, M. L.: Gridded National Inventory of U.S. Methane Emissions, *Environ. Sci. Technol.*, 50, 13123–13133, <https://doi.org/10.1021/acs.est.6b02878>, 2016.
- 645 Maasackers, J. D., Jacob, D. J., Sulprizio, M. P., Scarpelli, T. R., Nesser, H., Sheng, J.-X., Zhang, Y., Hersher, M., Bloom, A. A., Bowman, K. W., Worden, J. R., Janssens-Maenhout, G., and Parker, R. J.: Global distribution of methane emissions, emission trends, and OH concentrations and trends inferred from an inversion of GOSAT satellite data for 2010–2015, *Atmospheric Chemistry and Physics*, 19, 7859–7881, <https://doi.org/10.5194/acp-19-7859-2019>, 2019.
- 645 Maasackers, J. D., Jacob, D. J., Sulprizio, M. P., Scarpelli, T. R., Nesser, H., Sheng, J., Zhang, Y., Lu, X., Bloom, A. A., Bowman, K. W., Worden, J. R., and Parker, R. J.: 2010–2015 North American methane emissions, sectoral contributions, and trends: a high-resolution inversion of GOSAT observations of atmospheric methane, *Atmospheric Chemistry and Physics*, 21, 4339–4356, <https://doi.org/10.5194/acp-21-4339-2021>, 2021.



- 650 Maasackers, J. D., McDuffie, E. E., Sulprizio, M. P., Chen, C., Schultz, M., Brunelle, L., Thrush, R., Steller, J., Sherry, C., Jacob, D. J., Jeong, S., Irving, B., and Weitz, M.: A Gridded Inventory of Annual 2012–2018 U.S. Anthropogenic Methane Emissions, *Environ. Sci. Technol.*, *57*, 16276–16288, <https://doi.org/10.1021/acs.est.3c05138>, 2023.
- 655 Miller, S. M., Wofsy, S. C., Michalak, A. M., Kort, E. A., Andrews, A. E., Biraud, S. C., Dlugokencky, E. J., Eluszkiewicz, J., Fischer, M. L., Janssens-Maenhout, G., Miller, B. R., Miller, J. B., Montzka, S. A., Nehrkorn, T., and Sweeney, C.: Anthropogenic emissions of methane in the United States, *Proceedings of the National Academy of Sciences*, *110*, 20018–20022, <https://doi.org/10.1073/pnas.1314392110>, 2013.
- 660 National Centers for Environmental Information (NCEI): Climate at a Glance | Statewide Time Series, <https://www.ncei.noaa.gov/access/monitoring/climate-at-a-glance/statewide/time-series/3/pcp/3/8/2019-2025>, last access: 30 December 2025.
- 665 Nesser, H., Jacob, D. J., Maasackers, J. D., Scarpelli, T. R., Sulprizio, M. P., Zhang, Y., and Rycroft, C. H.: Reduced-cost construction of Jacobian matrices for high-resolution inversions of satellite observations of atmospheric composition, *Atmospheric Measurement Techniques*, *14*, 5521–5534, <https://doi.org/10.5194/amt-14-5521-2021>, 2021.
- 670 Nesser, H., Jacob, D. J., Maasackers, J. D., Lorente, A., Chen, Z., Lu, X., Shen, L., Qu, Z., Sulprizio, M. P., Winter, M., Ma, S., Bloom, A. A., Worden, J. R., Stavins, R. N., and Randles, C. A.: High-resolution US methane emissions inferred from an inversion of 2019 TROPOMI satellite data: contributions from individual states, urban areas, and landfills, *Atmospheric Chemistry and Physics*, *24*, 5069–5091, <https://doi.org/10.5194/acp-24-5069-2024>, 2024.
- 675 Nesser, H., Bowman, K. W., Thill, M. D., Varon, D. J., Randles, C. A., Tewari, A., Cardoso-Saldaña, F. J., Reidy, E., Maasackers, J. D., and Jacob, D. J.: Predicting and correcting the influence of boundary conditions in regional inverse analyses, *Geoscientific Model Development*, *18*, 9279–9291, <https://doi.org/10.5194/gmd-18-9279-2025>, 2025.
- 680 New Mexico Oil Conservation Commission: NM Natural Gas Waste Rule, New Mexico Administrative Code, 19.15.27.8 NMAC, 2021.
- 685 Omara, M., Himmelberger, A., MacKay, K., Williams, J. P., Benmergui, J., Sargent, M., Wofsy, S. C., and Gautam, R.: Constructing a measurement-based spatially explicit inventory of US oil and gas methane emissions (2021), *Earth System Science Data*, *16*, 3973–3991, <https://doi.org/10.5194/essd-16-3973-2024>, 2024.
- 685 Pendergrass, D. C., Jacob, D. J., Balasus, N., Estrada, L., Varon, D. J., East, J. D., He, M., Mooring, T. A., Penn, E., Nesser, H., and Worden, J. R.: Trends and seasonality of 2019–2023 global methane emissions inferred from a localized ensemble transform Kalman filter (CHEEREIO v1.3.1) applied to TROPOMI satellite observations, *Atmospheric Chemistry and Physics*, *25*, 14353–14369, <https://doi.org/10.5194/acp-25-14353-2025>, 2025.
- 690 Penn, E., D.H. Cusworth, K. Howell, K. O’Neill, T.R. Scarpelli, Z. Chen, R.A. Field, C.Ö. Karacan, E. Roy, and D.J. Jacob, Remote sensing enables basin-scale inventories of coal mine methane, submitted to *Environ. Sci. Technol.*, 2025.
- 695 Pennsylvania DEP: 2025 Pennsylvania Greenhouse Gas Inventory Report, Pennsylvania Department of Environmental Protection, 2025.
- 695 Randerson, J. T., Van Der Werf, G. R., Giglio, L., Collatz, G. J., and Kasibhatla, P. S.: Global Fire Emissions Database, Version 4.1 (GFEDv4), ORNL DAAC, <https://doi.org/10.3334/ORNLDAAC/1293>, 2017.
- Rodgers, C. D.: *Inverse Methods for Atmospheric Sounding: Theory and Practice*, WORLD SCIENTIFIC, <https://doi.org/10.1142/3171>, 2000.



- 700 Runkle, B. R. K., Suvočarev, K., Reba, M. L., Reavis, C. W., Smith, S. F., Chiu, Y.-L., and Fong, B.: Methane Emission Reductions from the Alternate Wetting and Drying of Rice Fields Detected Using the Eddy Covariance Method, *Environ. Sci. Technol.*, 53, 671–681, <https://doi.org/10.1021/acs.est.8b05535>, 2019.
- 705 Saunois, M., Martinez, A., Poulter, B., Zhang, Z., Raymond, P. A., Regnier, P., Canadell, J. G., Jackson, R. B., Patra, P. K., Bousquet, P., Ciais, P., Dlugokencky, E. J., Lan, X., Allen, G. H., Bastviken, D., Beerling, D. J., Belikov, D. A., Blake, D. R., Castaldi, S., Crippa, M., Deemer, B. R., Dennison, F., Etiope, G., Gedney, N., Höglund-Isaksson, L., Holgerson, M. A., Hopcroft, P. O., Hugelius, G., Ito, A., Jain, A. K., Janardanan, R., Johnson, M. S., Kleinen, T., Krummel, P. B., Lauerwald, R., Li, T., Liu, X., McDonald, K. C., Melton, J. R., Mühle, J., Müller, J., Murguía-Flores, F., Niwa, Y., Noce, S., Pan, S., Parker, R. J., Peng, C., Ramonet, M., Riley, W. J., Rocher-Ros, G., Rosentretter, J. A., Sasakawa, M., Segers, A., Smith, S. J., Stanley, E. H., Thanwerdas, J., Tian, H., Tsuruta, A., Tubiello, F. N., Weber, T. S., van der Werf, G. R., Worthy, D. E. J., Xi, Y., Yoshida, Y., Zhang, W., Zheng, B., Zhu, Q., Zhu, Q., and Zhuang, Q.: Global Methane Budget 2000–2020, *Earth System Science Data*, 17, 1873–1958, <https://doi.org/10.5194/essd-17-1873-2025>, 2025.
- 715 Scarpelli, T. R., Jacob, D. J., Villasana, C. A. O., Hernández, I. F. R., Moreno, P. R. C., Alfaro, E. A. C., García, M. Á. G., and Zavala-Araiza, D.: A gridded inventory of anthropogenic methane emissions from Mexico based on Mexico’s national inventory of greenhouse gases and compounds, *Environ. Res. Lett.*, 15, 105015, <https://doi.org/10.1088/1748-9326/abb42b>, 2020.
- 720 Scarpelli, T. R., Jacob, D. J., Moran, M., Reuland, F., and Gordon, D.: A gridded inventory of Canada’s anthropogenic methane emissions, *Environ. Res. Lett.*, 17, 014007, <https://doi.org/10.1088/1748-9326/ac40b1>, 2022.
- 725 Schneising, O., Burrows, J. P., Dickerson, R. R., Buchwitz, M., Reuter, M., and Bovensmann, H.: Remote sensing of fugitive methane emissions from oil and gas production in North American tight geologic formations, *Earth’s Future*, 2, 548–558, <https://doi.org/10.1002/2014EF000265>, 2014.
- 730 Schneising, O., Buchwitz, M., Reuter, M., Vanselow, S., Bovensmann, H., and Burrows, J. P.: Remote sensing of methane leakage from natural gas and petroleum systems revisited, *Atmospheric Chemistry and Physics*, 20, 9169–9182, <https://doi.org/10.5194/acp-20-9169-2020>, 2020.
- 735 Schuldt, K. N., Aalto, T., Andrade, M., Andrews, A., Apadula, F., Arduini, J., Arnold, S., Baier, B., Bartyzel, J., Bergamaschi, P., Biermann, T., Biraud, S. C., Blanc, P.-E., Boenisch, H., Brailsford, G., Brand, W. A., Brunner, D., Bui, T. P., Burban, B., Báni, L., Calzolari, F., Chang, C. S., Chen, H., Chmura, L., Climadat, S., Colomb, A., Condori, L., Conen, F., Conil, S., Couret, C., Cristofanelli, P., Cuevas, E., Curcoll, R., Daube, B., Davis, K. J., De Mazière, M., Dean-Day, J. M., Della Coletta, J., Delmotte, M., Desai, A., Di Iorio, T., DiGangi, J. P., DiGangi, E., Elsasser, M., Emmenegger, L., Forster, G., Frumau, A., Fuente-Lastra, M., Galkowski, M., Gatti, L. V., Gehrlein, T., Gerbig, C., Gheusi, F., Gloor, E., Goto, D., Hammer, S., Hanisco, T. F., Haszpra, L., Hatakka, J., Heimann, M., Heliasz, M., Heltai, D., Henne, S., Hensen, A., Hermans, C., Hermansen, O., Hoheisel, A., Holst, J., Iraci, L. T., Ivakhov, V., Jaffe, D. A., Jordan, A., Joubert, W., Kang, H.-Y., Karion, A., Kazan, V., Keeling, R. F., Keronen, P., Kers, B., Kim, J., Klausen, J., Kneuer, T., Ko, M.-Y., Kolari, P., Kominkova, K., Kort, E., Kozlova, E., Krummel, P. B., Kubistin, D., Kulawik, S. S., Kumps, N., Labuschagne, C., Lan, X., Langenfelds, R. L., Lanza, A., Laurent, O., Laurila, T., Lauvaux, T., Lavric, J., et al.: Multi-laboratory compilation of atmospheric methane data for the period 1981–2024, <https://doi.org/10.25925/20241001>, 2024.
- 740 Shen, L., Gautam, R., Omara, M., Zavala-Araiza, D., Maasackers, J. D., Scarpelli, T. R., Lorente, A., Lyon, D., Sheng, J., Varon, D. J., Nesser, H., Qu, Z., Lu, X., Sulprizio, M. P., Hamburg, S. P., and Jacob, D. J.: Satellite quantification of oil and natural gas methane emissions in the US and Canada including contributions from individual basins, *Atmospheric Chemistry and Physics*, 22, 11203–11215, <https://doi.org/10.5194/acp-22-11203-2022>, 2022.



750 Shen, L., Jacob, D. J., Gautam, R., Omara, M., Scarpelli, T. R., Lorente, A., Zavala-Araiza, D., Lu, X., Chen, Z., and Lin, J.:
National quantifications of methane emissions from fuel exploitation using high resolution inversions of satellite
observations, *Nat Commun*, 14, 4948, <https://doi.org/10.1038/s41467-023-40671-6>, 2023.

755 Sheng, J.-X., Jacob, D. J., Turner, A. J., Maasakkers, J. D., Benmergui, J., Bloom, A. A., Arndt, C., Gautam, R., Zavala-
Araiza, D., Boesch, H., and Parker, R. J.: 2010–2016 methane trends over Canada, the United States, and Mexico observed
by the GOSAT satellite: contributions from different source sectors, *Atmospheric Chemistry and Physics*, 18, 12257–12267,
<https://doi.org/10.5194/acp-18-12257-2018>, 2018.

760 Somkuti, P., McGarragh, G. M., O’Dell, C., Di Noia, A., Vogel, L., Crowell, S., Ott, L. E., and Bösch, H.: Surface
reflectance biases in XCH₄ retrievals from the 2.3 μm band are enhanced in the presence of aerosols, *Atmospheric
Measurement Techniques Discussions*, 1–20, <https://doi.org/10.5194/amt-2024-145>, 2025.

765 Turner, A. J., Jacob, D. J., Wecht, K. J., Maasakkers, J. D., Lundgren, E., Andrews, A. E., Biraud, S. C., Boesch, H.,
Bowman, K. W., Deutscher, N. M., Dubey, M. K., Griffith, D. W. T., Hase, F., Kuze, A., Notholt, J., Ohyama, H., Parker,
R., Payne, V. H., Sussmann, R., Sweeney, C., Velazco, V. A., Warneke, T., Wennberg, P. O., and Wunch, D.: Estimating
global and North American methane emissions with high spatial resolution using GOSAT satellite data, *Atmospheric
Chemistry and Physics*, 15, 7049–7069, <https://doi.org/10.5194/acp-15-7049-2015>, 2015.

770 Turner, A. J., Jacob, D. J., Benmergui, J., Wofsy, S. C., Maasakkers, J. D., Butz, A., Hasekamp, O., and Biraud, S. C.: A
large increase in U.S. methane emissions over the past decade inferred from satellite data and surface observations,
Geophysical Research Letters, 43, 2218–2224, <https://doi.org/10.1002/2016GL067987>, 2016.

775 Twyman, M., Hill, S., Banta, K., and Billingsley, R.: 2023 Colorado Statewide Inventory of Greenhouse Gas Emissions and
Sinks, 2024.

780 U.S. EIA: Natural gas gross withdrawals and production,
https://www.eia.gov/dnav/ng/ng_prod_sum_a_epg0_vgm_mmc_f_a.htm, 2025.

U.S. Greenhouse Gas Center: <https://earth.gov/ghgcenter>, last access: 2 May 2025.

785 Greenhouse Gas Reporting Program (GHGRP): <https://www.epa.gov/ghgreporting>, last access: 4 December 2025.

790 USDA NASS: Quick Stats Database, <https://quickstats.nass.usda.gov/>, 2025.

785 Varon, D. J., Jacob, D. J., Sulprizio, M., Estrada, L. A., Downs, W. B., Shen, L., Hancock, S. E., Nesser, H., Qu, Z., Penn,
E., Chen, Z., Lu, X., Lorente, A., Tewari, A., and Randles, C. A.: Integrated Methane Inversion (IMI 1.0): a user-friendly,
cloud-based facility for inferring high-resolution methane emissions from TROPOMI satellite observations, *Geoscientific
Model Development*, 15, 5787–5805, <https://doi.org/10.5194/gmd-15-5787-2022>, 2022.

790 Varon, D. J., Jacob, D. J., Hmiel, B., Gautam, R., Lyon, D. R., Omara, M., Sulprizio, M., Shen, L., Pendergrass, D., Nesser,
H., Qu, Z., Barkley, Z. R., Miles, N. L., Richardson, S. J., Davis, K. J., Pandey, S., Lu, X., Lorente, A., Borsdorff, T.,
Maasakkers, J. D., and Aben, I.: Continuous weekly monitoring of methane emissions from the Permian Basin by inversion
of TROPOMI satellite observations, *Atmospheric Chemistry and Physics*, 23, 7503–7520, <https://doi.org/10.5194/acp-23-7503-2023>, 2023.

795 Varon, D. J., Jacob, D. J., Estrada, L. A., Balasus, N., East, J. D., Pendergrass, D. C., Chen, Z., Sulprizio, M., Omara, M.,
Gautam, R., Barkley, Z. R., Saldaña, F. J. C., Reidy, E. K., Kamdar, H., Sherwin, E. D., Biraud, S. C., Jervis, D., Pandey, S.,
Worden, J. R., Bowman, K. W., Maasakkers, J. D., and Kleinberg, R. L.: Seasonality and Declining Intensity of Methane



Emissions from the Permian and Nearby US Oil and Gas Basins, *Environ. Sci. Technol.*,

<https://doi.org/10.1021/acs.est.5c08745>, 2025.

- 800 Wang, X., Jacob, D. J., Nesser, H., Balasus, N., Estrada, L., Sulprizio, M., Cusworth, D. H., Scarpelli, T. R., Chen, Z., East, J. D., and Varon, D. J.: Quantifying urban and landfill methane emissions in the United States using TROPOMI satellite data, <https://doi.org/10.48550/arXiv.2505.10835>, 2025.
- 805 Worden, J. R., Cusworth, D. H., Qu, Z., Yin, Y., Zhang, Y., Bloom, A. A., Ma, S., Byrne, B. K., Scarpelli, T., Maasakkers, J. D., Crisp, D., Duren, R., and Jacob, D. J.: The 2019 methane budget and uncertainties at 1° resolution and each country through Bayesian integration Of GOSAT total column methane data and a priori inventory estimates, *Atmospheric Chemistry and Physics*, 22, 6811–6841, <https://doi.org/10.5194/acp-22-6811-2022>, 2022.
- 810 Yuan, B., Kaser, L., Karl, T., Graus, M., Peischl, J., Campos, T. L., Shertz, S., Apel, E. C., Hornbrook, R. S., Hills, A., Gilman, J. B., Lerner, B. M., Warneke, C., Flocke, F. M., Ryerson, T. B., Guenther, A. B., and de Gouw, J. A.: Airborne flux measurements of methane and volatile organic compounds over the Haynesville and Marcellus shale gas production regions, *Journal of Geophysical Research: Atmospheres*, 120, 6271–6289, <https://doi.org/10.1002/2015JD023242>, 2015.
- 815 Zhang, Y., Gautam, R., Pandey, S., Omara, M., Maasakkers, J. D., Sadavarte, P., Lyon, D., Nesser, H., Sulprizio, M. P., Varon, D. J., Zhang, R., Houweling, S., Zavala-Araiza, D., Alvarez, R. A., Lorente, A., Hamburg, S. P., Aben, I., and Jacob, D. J.: Quantifying methane emissions from the largest oil-producing basin in the United States from space, *Science Advances*, 6, eaaz5120, <https://doi.org/10.1126/sciadv.aaz5120>, 2020.
- 820 Zhao, C., Andrews, A. E., Bianco, L., Eluszkiewicz, J., Hirsch, A., MacDonald, C., Nehr Korn, T., and Fischer, M. L.: Atmospheric inverse estimates of methane emissions from Central California, *Journal of Geophysical Research: Atmospheres*, 114, <https://doi.org/10.1029/2008JD011671>, 2009.